Time-resolved imaging and immobilization study of biomaterials on hydrophobic and superhydrophobic surfaces by means of laser-induced forward transfer

2014 Laser Phys. Lett. 11 105603

(http://iopscience.iop.org/1612-202X/11/10/105603)

IOP Publishing | Astro Ltd
Laser Physics Letters
Laser Phys. Lett. **11** (2014) 105603 (8pp)
doi:10.1088/1612-2011/11/10/105603

Time-resolved imaging and immobilization study of biomaterials on hydrophobic and superhydrophobic surfaces by means of laser-induced forward transfer

Christos Boutopoulos[1], Marianneza Chatzipetrou[1], Athanasios G Papathanasiou[2] and Ioanna Zergioti[1]

[1] School of Applied Mathematical and Physical Sciences, National Technical University of Athens, GR-15780 Athens, Greece
[2] School of Chemical Engineering, National Technical University of Athens, GR-15780 Athens, Greece

E-mail: zergioti@central.ntua.gr

Received 20 November 2013, revised 1 July 2014
Accepted for publication 28 July 2014
Published 22 August 2014

Abstract

In this work, we present the generation of high velocity liquid jets of a photosynthetic biomaterial in buffer solution (i.e. thylakoid membranes) and a test solution, using the laser-induced forward transfer (LIFT) technique. The high impact pressure of the collision of the jets on solid substrates, ranging from 0.045 MPa–35 MPa, resulted in strong physical immobilization of the photosynthetic biomaterial on superhydrophobic (SH) poly(methyl methacrylate) (PMMA) surfaces and hydrophobic gold surfaces. The immobilization efficiency was evaluated by fluorescence microscopy, while time-resolved imaging of the LIFT process was carried out to study the corresponding LIFT dynamics. The results show that this simple, direct and chemical-linkers-free immobilization technique is valuable for several biosensors and microfluidic applications since it can be applied to a variety of hydrophobic and SH substrates, leading to the selective immobilization of the biomaterials, due to the high spatial printing resolution of the LIFT technique.

Keywords: laser induced forward transfer, laser immobilization of biomaterials, time-resolved imaging of LIFT

S Online supplementary data available from stacks.iop.org/LPL/11/105603/mmedia

(Some figures may appear in colour only in the online journal)

1. Introduction

Recently, a great effort has been directed towards the fabrication of superhydrophobic (SH) surfaces due to their wide range of applications including microfluidics [1], self-cleaning [2, 3] and liquid-repellent textiles [4, 5]. In the bio-applications field, the use of superhydrophobic surfaces and/or smart substrates of tunable wettability offer a great potential for developing micro-flow bioanalysis systems with miniaturized size and low power consumption [1, 6].

One of the most crucial steps in the fabrication of bioanalysis systems, like biosensors and microarrays, is the efficient immobilization of the probe biomolecules onto their surface. The sensitivity of such systems is directly linked with the stability and accessibility of the immobilized molecules. Several immobilization pathways have been developed including both chemical and physical procedures [7]. The chemical methods provide covalent bonds between the material and the immobilizing agent resulting in low leaking of the material during the analysis. However, the presence of additional surface functionalization steps in chemical immobilization procedures, is usually time consuming and demand special care of the involved chemical agents. In addition, the physical methods are mainly based on physical adsorption

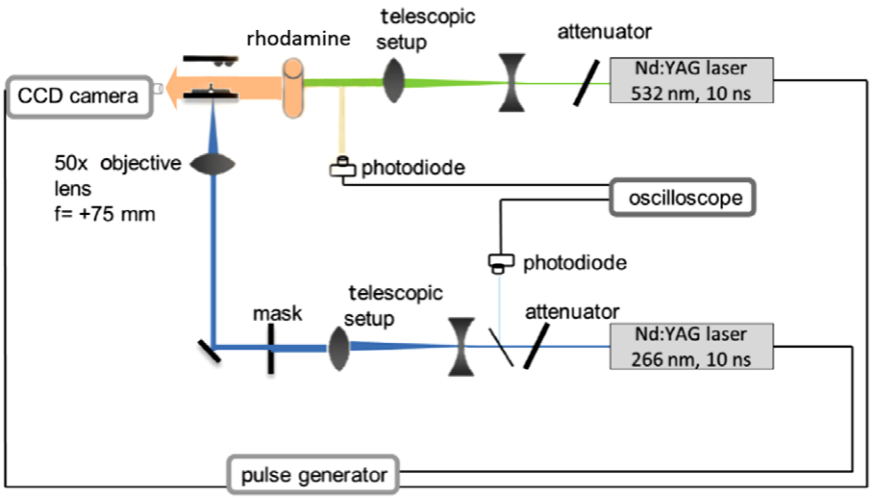

Figure 1. Schematic illustration of the laser induced forward transfer (LIFT) experimental setup and the pump–probe ultrafast imaging setup.

on specific substrates or the inclusion of the molecules into specific matrixes.

A physical and versatile immobilization technique has been recently demonstrated by our group for the development of biosensors for pesticides and polyphenol compounds detection [8, 9] based on the laser-induced forward transfer (LIFT) technique [10]. LIFT enables the controlled transfer of a thin film of a liquid or solid material, from a donor substrate to a receiving substrate by means of pulsed laser irradiation. Recently, LIFT has been successfully applied to a plethora of organic and inorganic materials including cells [11], proteins [12], DNA [13], metallic nanoparticle inks [14–16] and polymers [15, 17, 18] towards to the development of a variety of devices and applications [10].

A typical liquid phase LIFT donor substrate consists of a transparent carrier coated by a thin irradiation absorption layer on which the liquid film has been coated. The liquid material ejection is initiated by the generation of a high pressure vapor pocket at the irradiation absorbing layer–liquid film interface due to the localized laser energy delivery. Several time-resolved imaging studies of the LIFT process, including vapor pocket expansion and liquid ejection [16, 19–22], reveal that under the optimum laser fluence, the generated vapor pocket expands, resulting in the formation of a long and stable jet [16, 19, 22]. The impingement of the jet on the receiving substrate causes accumulation of liquid at the impact position, forming of a drop. The importance of the smooth and low-velocity jetting behavior in high spatial resolution LIFT printing is highlighted in most of the works dealing with LIFT on hydrophilic substrates. Recently, it has been shown that high-velocity LIFT generated jets present remarkable ability to induce wetting transitions on SH substrates, indicating a high potential for achieving biomaterials' immobilization on these surfaces [23], opening a new route on selective immobilization of biomaterials on liquid repellent surfaces. It is worth mentioning that most of the liquids are repelled from SH surfaces which can remain clean from any other substance except a desired immobilized biomaterial.

Considering applications of microfluidic and lab-on-chip systems, where the immobilization method should provide a strong link between the probe molecules and the substrate in order to withstand the flow conditions, we applied LIFT to immobilize biomaterials on plasma etched SH poly(methyl metha-crylate) (PMMA) surfaces. The selection of the PMMA surfaces is motivated by the specific advantages (i.e. low cost, optical transparency, simple fabrication, tunable wettability) and the popularity of the PMMA surfaces in microfluidic devices fabrication [24]. In order to study the immobilization technique we performed ultrafast dynamical studies of the LIFT process by using a pump–probe imaging methodology and a test liquid. The morphology and the velocity of the LIFT generated jets were correlated with the immobilization efficiency of photosynthetic biomaterial on a SH rough PMMA surface and a hydrophobic rough gold electrode. The immobilization of the photosynthetic biomaterial was confirmed by fluorescence microscopy, while control experiments were also performed using pipette deposition.

2. Materials and methods

The experimental setup used in this study is depicted in figure 1. Laser printing of the test liquid and the biomaterial solutions was achieved by using a pulsed Nd:YAG (yttrium aluminium garnet) laser (266 nm wavelength, 10 ns pulse duration) and a mask projection optical setup composed of a beam expander, a variable circular mask, an attenuator and a converging lens. The imaging system was adjusted to a demagnification factor of 5 (1/M) resulting to a spot size at the imaging plane ranging from 80 μm–130 μm. The liquid jet was created on the donor and subsequently collided on the receiving surface by the action of a single laser pulse.

2.1. Donor substrates

The donor substrates were prepared by drop casting 30 μL of the test liquid or the biomaterial solution on a quartz support which is coated with a 40 nm titanium laser-absorbing layer. This resulted to the formation of liquid film with a thickness of about 60 μm on the support.

The test liquid used in the current study was a 1.0 M potassium phosphate buffer (0.5 M KH2PO4, 0.5 M K2HPO4,

pH 8), plus the sodium dodecyl sulfate surfactant diluted at a concentration of 2.0 mg ml^{-1}. The measured viscosity, η, of the test liquid was equal to 1.15 mPa s. In order to prepare the biomaterial solution thylakoid membranes were extracted from fresh spinach leaves *(Spinaceaoleracea L)* using a protocol that has been described in detail in previous work [9]. In the final step, thylakoid membranes were re-suspended in a buffer containing 25 mM 2-(N-morpholino)ethanesulfonic acid (MES) pH = 6.0, 70 mM sucrose, and 15 mM NaCl. The final concentration of the thylakoid solution on the donor substrate was 7.6 mg ml^{-1}.

2.2. Receiving substrates

The SH substrates were prepared by oxygen plasma etching followed by fluorocarbon plasma deposition on 2 mm thick poly(methyl methacrylate) (PMMA) substrates, which produce hierarchical randomly rough SH surfaces. The preparation of the SH substrates has been previously described in detail [25]. Surface roughness protrusions are of mean diameter 310 nm ± 90 nm, mean spacing 420 nm ± 31 nm, and mean height 860 nm ± 30 nm. The gold screen printed electrodes (SPEs) were purchased by DropSens SL Spain (ref. C223BT). LIFT immobilization of the thylakoid biomaterial was performed on the gold working electrode (1.6 mm diameter) of the SPEs. The rms roughness of the gold electrode surface was measured by atomic force microscopy to be 560 ± 3 nm.

The receiving substrates were fixed in a 'face down' configuration opposite to the donor substrate; the distance between the donor and receiving substrates was fixed at about 300 μm.

2.3. Time-resolved imaging setup

Side view time-resolved imaging of the printing process was conducted using the pump–probe experimental setup shown in figure 1. By means of a second Nd:YAG laser (at 532 nm wavelength and 10 ns pulse duration) a fluorescence dye (rhodamine solution) was pumped onto a transparent container placed on the camera axis. For capturing the shadowgraphic images a CCD camera (Unibrain Fire-i 810) has been used, equipped with a 50× long working distance objective lens and placed perpendicular to the laser printing axis. The triggering of the CCD camera as well as time synchronization of the pump and probe laser pulses was achieved by using a pulse delay generator (DG535, Stanford Research Systems), which allowed setting the delay between the printing (pump) and illuminating (probe) laser pulses with a temporal resolution of few ns. The exact delay between the two pulses was measured using two photodiodes connected to an oscilloscope.

Series of images were taken by moving the donor-receiving substrate assembly in the *x*- or *y*-direction so as an unused region was irradiated for each image frame. Three to five images were taken for each delay time to ensure reproducibility. The analysis of the images was carried out by using the ImageJ software to extract the front distance of the ejected material as a function of the time.

2.4. Immobilization experiments

In what follows, we consider as immobilization the case where the biomolecules are deposited and adsorbed in the tested surfaces (gold electrodes or the rough PMMA surfaces) and can remain active after the rinsing steps. In particular, a washing protocol was applied on each receiving substrate after the laser induced printing of the thylakoid biomaterial. This consists of a 5 min rinsing with a buffer containing: tricine 20 mM pH 7.8, sucrose 70 mM, NaCl 15 mM, $MgCl_2$ 5 mM, which is a common measuring buffer used in amperometric characterization of thylakoid-based sensors [9]. Afterwards, the samples were kept at 4 °C under dark conditions for 4 h, until the fluorescence microscopy observation. The natural fluorescence of the chlorophylls enabled the evaluation of the thylakoids immobilization without using artificial tags. Control experiments were carried out by using a pipette to deposit 1 μL of the thylakoid solution on the receiving substrates.

The fluorescence images were recorded by a Leica fluorescence microscope. All the sample surfaces were captured and recorded by keeping the same fixed parameters such as the gain, exposure time and filter values of the fluorescent microscope. For the quantification of the immobilization efficacy of the photosynthetic material, the photographs taken with the use of the fluorescent microscope were processed with the use of ImageJ software. The change in fluorescence intensity for each spot was determined by the following formula:

$$\text{Specified mean OD} - \text{Background mean OD}$$

OD, in the context of the data presented, corresponds to the fluorescence signal intensity of each spot in arbitrary units and not to optical absorbance. Fluorescence intensity for each spot was calculated by averaging the gray intensity value across its entire surface. Reference areas of each sample (no laser printing or pipette printing) were used to calculate the background OD. Care was also taken so as not to saturate the images that would render fluorescence qualitative results non-instructive.

3. Results and discussion

3.1. Time-resolved imaging of LIFT dynamics

In the first part of this work, we have investigated the LIFT dynamics of the test liquid for various laser fluences. Figures 2(*a*)–(*c*) show snapshots of liquid material ejection for laser fluence ranging from 430 mJ cm^{-2} to 930 mJ cm^{-2}. As we observe, for the entire laser fluence range, the ejection of the liquid material is initiated by the formation of a cavitation bubble. The dynamic growth and expansion of the latter strongly depends on the laser fluence.

The driving force for the formation of the bubble originates from the localized energy delivery at the titanium layer/liquid layer interface following the laser irradiation. In particular, the laser pulse energy is absorbed within the first ~17 nm of the 40 nm thick titanium layer [26]. At 430 mJ cm^{-2}, heat conduction is considered as the main mechanism for the energy transfer to the underlying liquid layer and the concomitant creation of vapor pressure through liquid vaporization. Figure 2(*a*) shows several snapshots of the cavitation bubble formation

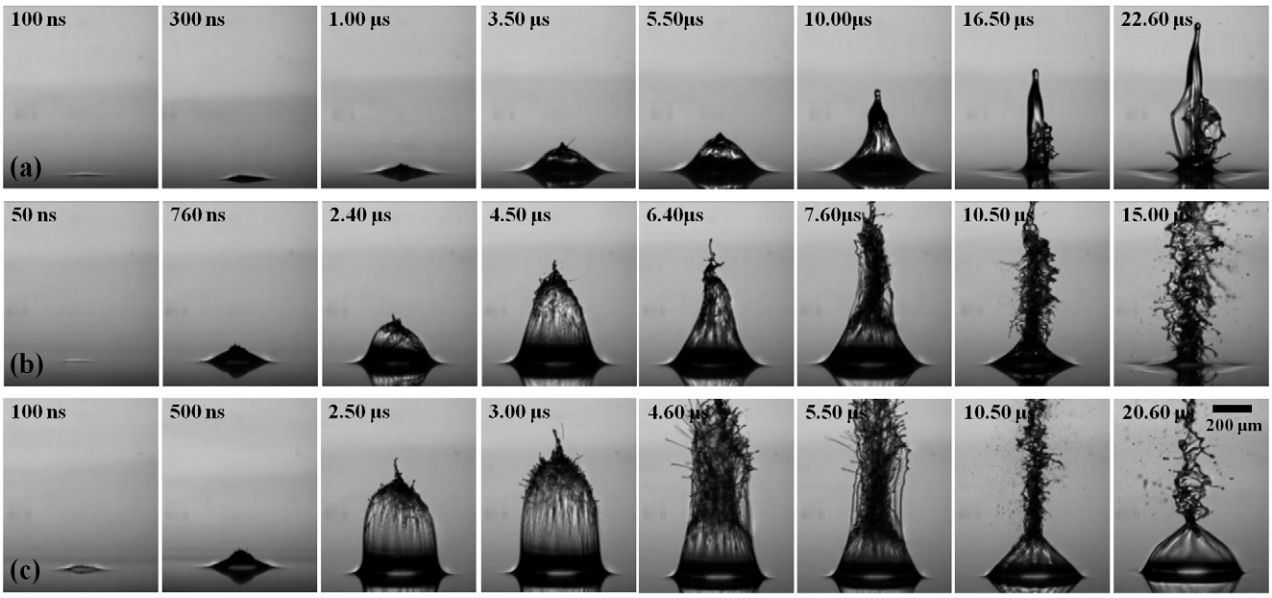

Figure 2. Shadowgraphic time-resolved images of the test liquid ejection under various laser fluences: (*a*) 430 mJ cm^{-2}, (*b*) 600 mJ cm^{-2} and (*c*) 930 mJ cm^{-2}. Pictures were captured at different time delays with respect to the pump laser pulse.

and expansion at 430 mJ cm^{-2}. At around 300 ns after the laser pulse the cavitation bubble size is exceeding the initial liquid film thickness (~60 μm) resulting to a displacement of its free surface. The expansion phase lasts about 10 μs, where the high pressure bubble remains sealed by the underlying liquid film. As the kinetic energy of the expanding bubble overcomes the pull off surface tension and viscous forces, part of the liquid film detaches from the surface forming a jet.

Ablation of the intermediate titanium layer is observed for LIFT at 600 mJ cm^{-2} (figure 2(*b*)) resulting in a confined, high temperature and pressure plasma. Optical emission of the plasma is observed in figure 2(*b*) (also in figures 2(*c*) and 3), where a bright spot is visible at the irradiation area. Despite lasting few tenths of ns [27], plasma emission is visible in late frames due to the superposition imaging technique (the exposure time for each frame was 1 ms). Due to plasma relaxation and collision, the test liquid is rapidly heated resulting in a dynamic cavitation bubble whose expansion forces the liquid at the periphery of the irradiated area. As a result, a significant secondary expulsion of liquid at the periphery of the irradiated area is observed, having conical (figure 2(*b*)) or cylindrical (figures 2(*c*) and 3) shape, depending on the laser fluence. This secondary liquid ejection lasts up to few tenths of μs. A video of the ejection dynamics at 930 mJ cm^{-2} can be found in the supplementary material (available online at stacks.iop.org/LPL/11/105603/mmedia).

For intermediate laser fluences (600 mJ cm^{-2}–930 mJ cm^{-2}), the ejected liquid at the periphery of the laser spot merges into a conical jet-like formation due to coherent forces and underpressure (i.e. rapid pressure release following the bubble explosion) in the cavity [28, 29]. Further increment of the laser fluence, up to the extreme value of 3.5 J cm^{-2}, results in supersonic material ejection and shock wave propagation (see inset in figure 3). At that laser fluence, the expanding cavitation bubble propels rabidly the overlying material resulting in cloud-like ejection morphology.

Figure 4 shows the dependence of the jet velocity on the laser fluence. Each velocity value was calculated by a linear fit of the liquid front vertical position dependence on the time. The calculated velocities vary from 10.5 ms^{-1} to 267 ms^{-1} for laser fluences ranging from 150 mJ cm^{-2}–1320 mJ cm^{-2}, respectively. For the extremely high laser fluence condition of 3.5 J cm^{-2}, the ejection velocity was calculated to be 795 ms^{-1} (i.e. ~2.3 times the supersonic threshold). Although high ejection velocity has the key role in LIFT immobilization of biomaterials, supersonic material ejection and shock wave propagation during LIFT have a catastrophic effect on the deposition quality [30, 31] and must be avoided. Therefore, the fluence range selected for our immobilization experiments lies well below the threshold for supersonic ejection.

When LIFT is performed under jet conditions (either smooth or turbulent), the high velocity impact of the liquid jet onto the receiving substrate generates an impact pressure at the substrate. We calculate the impact pressure using $P_{\mathrm{im}} = 1/2\rho u_{\mathrm{im}}^2$, where, u_{im}, is the impact velocity of the liquid jet and, ρ, is the density of the liquid [32]. Figure 4 also shows the dependence of the calculated impact pressure on the laser fluence considering the experimental defined ejection velocities (see the right axis). The impact pressure, vary from 0.045 MPa–35 MPa for laser fluences ranging from 150 mJ cm^{-2}–1320 mJ cm^{-2}, respectively. Notice that a 35 MPa impact pressure is achievable with a slightly turbulent jet. However, this value is about 30 times higher than the pressure attained with other conventional liquid printing/deposition methods. For instance, the maximum impact pressure for conventional ink jet printing is about 1 MPa, while a rain droplet (maximum speed of the order of 10 ms^{-1}) induces a dynamic pressure of 100 kPa during the impact.

As the laser generated droplet hits the rough superhydrophobic surface having a speed, u_{im}, the liquid-air interface

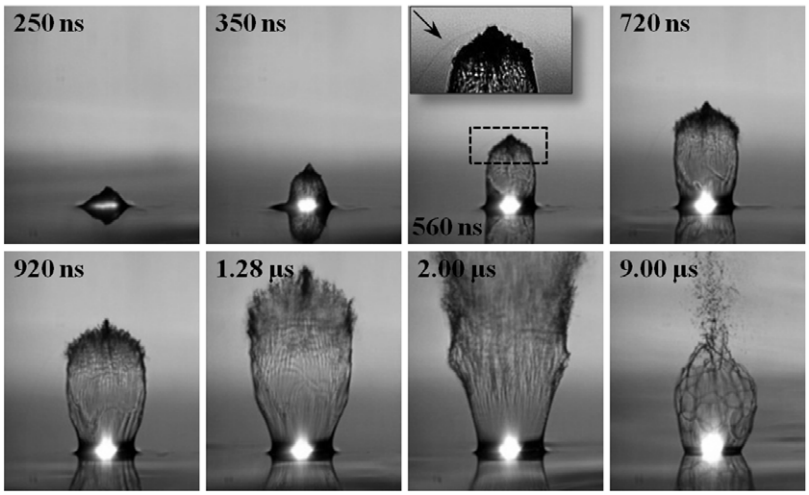

Figure 3. Shadowgraphic time-resolved images of the test liquid ejection for laser fluence of 3.5 J cm^{-2}. The inset picture shows a close up to the front material ejection and the black arrow points the shock wave expansion. The bright spot at the point of irradiation corresponds to the plasma emission produced by the titanium layer ablation.

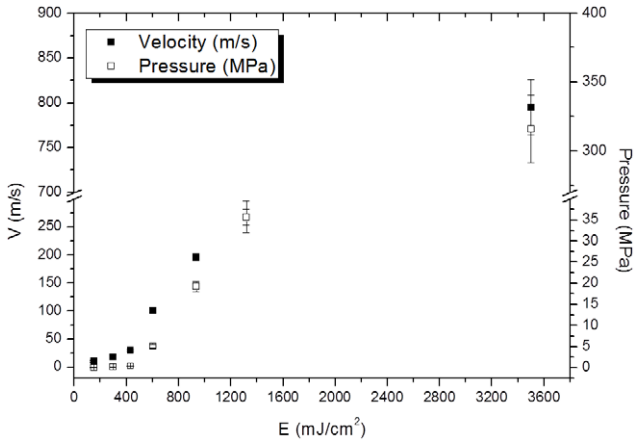

Figure 4. The calculated front velocity as a function of the laser fluence (left axis); the corresponding impact pressure as a function of the laser fluence (right axis). Velocity error bars correspond to the standard error of the linear fit over the material position dependence on time. Pressure error bars correspond to the velocity error propagation.

above the droplet is deformed when the impact pressure is higher than a critical Laplace pressure [33]. For a patterned surface, when the typical size of the roughness is smaller than the size of the sessile droplet, the Laplace pressure, P_L, inside the droplet reads [34]:

$$P_L = \frac{2\gamma}{R} \tag{1}$$

where γ is the air-liquid interfacial tension and R is the radius of curvature.

When the droop, δ, of the droplet in the valleys of the solid surface is considerably small, the Laplace pressure can be written as a function of γ, δ and L_{mean} [34] as follows:

$$P_L = \frac{16\gamma\delta}{L_{\text{mean}}^2} \tag{2}$$

where L_{mean} is the mean distance between the pillars of the substrate and the droop of the droplet (δ) is given by the function:

Droop of a droplet, sitting on a patterned surface.

$$\delta = \frac{L_{\text{mean}}^2}{8R} \tag{3}$$

where R is the radius of curvature of the droplet that can be found in the middle of two pillars that are diagonally across.

The critical Laplace pressure is the pressure at which the droplet removes the entrapped air from the surface and the droplet contacts the bottom of the cavities between the pillars. If the u_{im} is high enough and the corresponding impact pressure is higher than the critical Laplace pressure, the droplet touches the bottom of the rough surface leading to the complete wetting of the surface and thus the direct immobilization of the biomaterials. Considering that the droplet starts to penetrate to the roughness of the surface, when the impact pressure is equal or higher than the critical Laplace pressure, then the δ value is in the same order of magnitude or higher than the height of the pillars.

The critical Laplace pressure can be estimated analytically for periodically structured substrates but can be hardly calculated for randomly roughened SH surfaces. Nonetheless in this work, an estimation of the critical Laplace pressure is given. The Laplace pressure threshold has been calculated by using the mean distance between the pillars, L_{mean} (420 nm ± 30 nm), as geometric parameter. Our measurement showed that at the immobilization threshold i.e. when the droplet starts to penetrate to the roughness of the surface, the impact pressure is 1.2 MPa. Equating at this point the impact pressure with the Laplace pressure, the δ value is calculated to be 430 nm which is the half height of the pillars (432 nm ± 15 nm). According to this result, the droplet does not penetrate completely to the valleys of the surface, but penetrates enough so as to observe direct immobilization (figure 5).

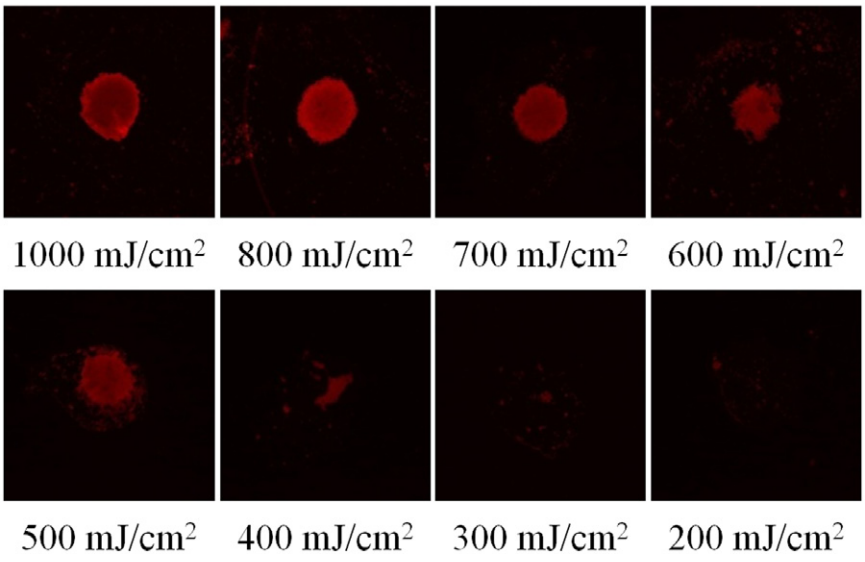

Figure 5. Fluorescence microscopy images of photosynthetic biomaterial spots on a superdydrophobic PMMA surface deposited by using LIFT. Progressive increment of the laser fluence revealed a laser fluence threshold of 500 mJ cm^{-2} for strong immobilization of the biomaterial onto the SH surface.

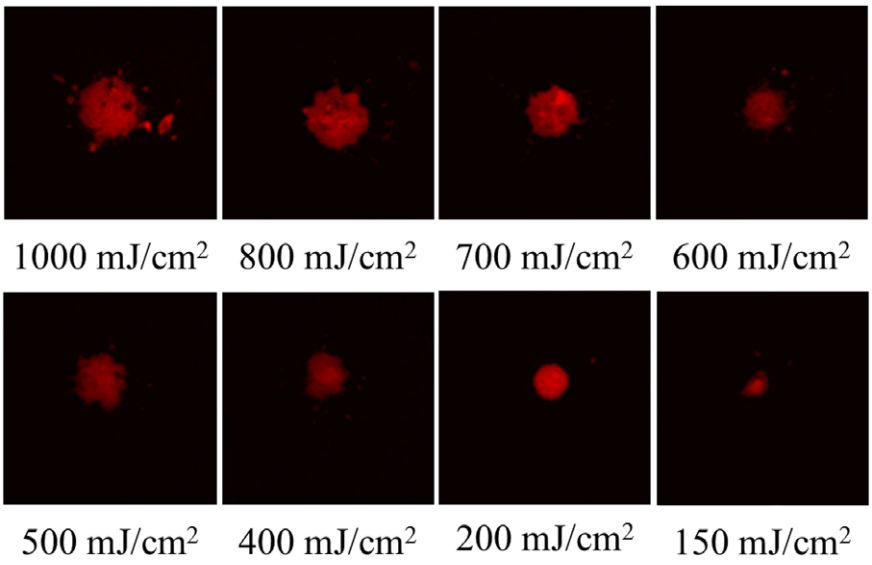

Figure 6. Fluorescence microscopy images of photosynthetic biomaterial spots on a rough gold SPE deposited by using LIFT. The direct laser immobilization threshold for the gold SPEs is 200 mJ cm^{-2}.

In addition when the impact pressure reaches 35 MPa, the droplet is considered to touch the bottom of the cavities and thus the radius of curvature tends to $L_{mean}/2$ [35]. The δ value in this case is approximately calculated to be 8 μm, which is much higher than the height of the pillars (865 nm ± 30 nm), leading to the complete wetting of the surface and thus the stronger absorption of the droplet to the surface.

For the gold substrates, the immobilization threshold according to figure 6 is found to be at lower laser energy fluences, which is explained due to the smaller geometrical surface details of the rough gold surface.

3.2. Biomaterials immobilization

Biomaterial immobilization tests, without any chemical linker, are conducted by using LIFT to transfer a solution containing photosynthetic material (i.e. thylakoid membranes extracted from spinach leaves) on plasma engineered superhydrophobic PMMA surfaces. Figure 5 shows fluorescence microscopy images of photosynthetic biomaterial spots deposited on a superhydrophobic PMMA by varying the laser fluence. For laser fluence ranging from 200 mJ cm^{-2} to 400 mJ cm^{-2}, negligible immobilization is observed. Indeed, the natural fluorescing biomaterial (red emission) was removed during the rinsing step, while some remaining weak fluorescence indicates the area of impact of the liquid jet during the LIFT process. The threshold value for the immobilization of the biomaterial drop onto the surface is 500 mJ cm^{-2}. Further increment of the laser fluence up to 1000 mJ cm^{-2}, resulted in the immobilization of uniform spots of the biomaterial onto the SH PMMA surface.

The observed immobilization efficiency of the LIFT method is mainly attributed to the high impact pressure

Table 1. Correlation of biomaterial immobilization efficiency on different substrates with the LIFT induced CA modulation.

Substrate	Pipette CA	Transition laser fluence threshold	Transition impact pressure threshold	LIFT CA saturation value*	Biomaterial immobilization
Rough PMMA	157 ± 3	~500 mJ cm^{-2}	~1.2 MPa	90 ± 5	Yes
Rough gold	90 ± 3	~200 mJ cm^{-2}	~0.07 MPa	24 ± 3	Yes

* Minimum CA value at high laser fluences (up to 1.3 J cm^{-2}).

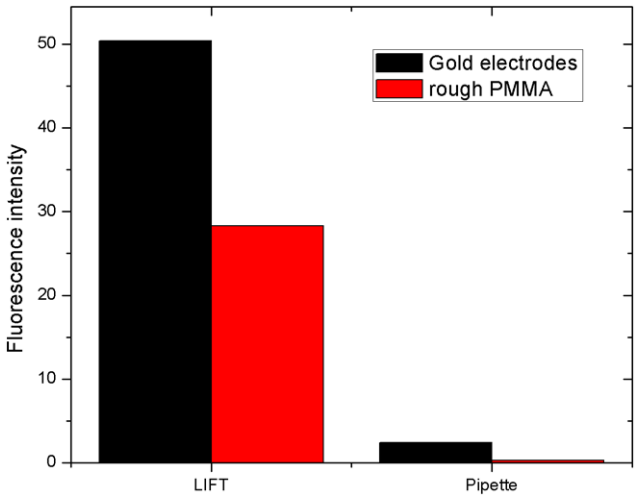

Figure 7. The fluorescence intensity of biomaterial spots immobilized by LIFT compared to the control pipette deposition method. Two different substrates were tested: hydrophobic gold electrodes and oxygen plasma engineered superhydrophobic PMMA.

induced by the high velocity collision of the liquid jets on the SH surface. The jet impact velocities for the test liquid at 150 mJ cm^{-2} and 1320 mJ cm^{-2} were 10.5 ms^{-1} and 267 ms^{-1}, respectively (figure 4), corresponding to an impact pressure ranging from 0.045 MPa to 35 MPa. At 500 mJ cm^{-2}, the impact pressure is estimated to be ~1.2 MPa, which can be considered as the minimum pressure required for forcing the biomaterial to penetrate into the roughness features of the rough PMMA surface [23].

A control experiment was also performed by using pipette to deposit a droplet of the thylakoid solution onto the SH PMMA surface. Thylakoid material detached from the surface during the washing step and thus very weak fluorescence intensity has been recorded. The comparison between LIFT and pipette immobilization efficiency (in terms of fluorescence intensity) is shown in figure 7. LIFT, above the laser fluence immobilization threshold, resulted in an almost seven-times higher binding efficiency compared to the control experiments.

The key role of the impact pressure in materials immobilization efficiency is demonstrated. Indeed, high impact pressure during LIFT process has been recently reported by our group to induce wetting transitions when applied to deposit droplets on SH PMMA surfaces [23]. In particular, LIFT deposited droplets presented an almost 60° lower contact angle (CA) compared to reference pipette deposited droplets on the same superhydrophobic surface, indicating transition from a non-wetting state to a highly wetting state. A high wettability state allows for achieving increased physical contact between the biomaterial and the effective surface area of the substrate and therefore significantly enhances the physical adsorption.

Similar immobilization results were also obtained when hydrophobic rough gold electrodes were used as test substrates (figure 6). Since the gold SPEs presented smaller roughness value (rms) and is not superhydrophobic like Teflon coated PMMA, the immobilization threshold is found at lower laser energy fluence (200 mJ cm^{-2}), where the impact pressure corresponds to 0.07 MPa which is much lower than the one needed (i.e. 1.2 MPa) to achieve immobilization on the SH PMMA surface. Fluorescence microscopy revealed that LIFT, above the laser fluence immobilization threshold, results in almost ten-times higher immobilization efficiency compared to control pipette experiment (figure 7). The poor thermodynamic robustness of the hydrophobic behavior compared to the SH PMMA surface is considered as the main reason for the observed lower threshold fluence for immobilization.

Contact angle measurements of the test liquid on both substrates under LIFT and pipette, confirmed the lower threshold for a wetting transition when gold surfaces were used (table 1). The threshold is defined as the minimum laser fluence for achieving a wetting transition, i.e. from superhydrophobic to hydrophobic state and hydrophobic to hydrophilic state for PMMA and gold surfaces, respectively.

The ability of oxygen plasma engineered PMMA surfaces to enhance protein adsorption has been extensively studied in the past [6, 36]. However, these studies deal with hydrophilic surfaces, where liquid drops penetrate the roughness spontaneously resulting in an enhanced physical adsorption process due to the high effective surface area of the rough substrates. It has also been demonstrated that SH surfaces present pronounced ability to suppress protein adsorption [6, 37]. Using the LIFT technique to produce high impact pressure of the biomaterial droplets on the SH surfaces we triggered a wetting transition, which lead to strong biomaterial immobilization. Strong, direct and selective immobilization of biomaterials on SH surfaces can benefit various microfluidic applications. For instance, the use of SH substrates with immobilized probe molecules for the realization microfluidic sensing devices can eliminate the non-controllable adsorption of target molecules. This is a crucial issue for applications that demand high sensitivity, such as pesticides detection, where the typical detection range lies within the nM scale.

4. Conclusions

We demonstrated the use of LIFT technique for achieving high and selective immobilization efficiency of thylakoid biomaterial on SH PMMA surfaces and hydrophobic rough surfaces without using chemical linkers. Time-resolved imaging

of the LIFT dynamics was performed to provide an insight to the impact pressure of the droplet, at the surface, leading to the physical immobilization technique. The generation of high impact pressure, up to35 MPa, of the LIFT generated liquid jets on the surfaces induced a wetting transition, which is considered as the dominant mechanism for the immobilization of the biomaterials. The use of SH substrates in biomicrofluidic devices finds a plurality of applications, which can be further benefited by the proposed approach since it provides a physical and high spatial resolution method to immobilize probe molecules onto their surface.

Acknowledgements

The authors kindly acknowledge funding from the European Research Council under the European Community's Seventh Framework Programme (FP7/ 2007–2013)/ERC Grant Agreement No. [240710] (AGP) The contribution of Dimitrios P Papageorgiou is acknowledged. Rough PMMA samples were fabricated in NCSR 'Demokritos,' followed by the expert advice of Dr E Gogolides and Dr A Tserepi. The authors would also like to acknowledge the contribution of E Rigana from B.R.F.A.A. for the fluorescent microscopy images and Dr M Massaouti for text editing corrections.

References

[1] Papageorgiou D P, Tsougeni K, Tserepi A and Gogolides E 2013 *Microfluid. Nanofluid.* **14** 247
[2] Marmur A 2004 *Langmuir* **20** 3517
[3] Patankar N 2004 *Langmuir* **20** 8209
[4] Deng B *et al* 2010 *Adv. Mater.* **22** 5473
[5] Zimmermann J, Reifler F A, Fortunato G, Gerhardt L-C and Seeger S 2008 *Adv. Funct. Mater.* **18** 3662
[6] Tsougeni K, Petrou P S, Papageorgiou D P, Kakabakos S E, Tserepi A and Gogolides E 2012 *Sensors Actuators* B **161** 216
[7] Barthelmebs L, Carpentier R and Rouillon R 2011 *Methods Mol. Biol.* **684** 247
[8] Boutopoulos C, Touloupakis E, Pezzotti I, Giardi M T and Zergioti I 2011 *Appl. Phys. Lett.* **98** 093703
[9] Touloupakis E, Boutopoulos C, Buonasera K, Zergioti I and Giardi M T 2012 *Anal. Bioanal. Chem.* **402** 3237
[10] Vorobyev A, Guo C, Sakata H, Wakaki M, Wang Q, Sametoglu V, Tsui Y Y, Nagel M and Lippert T 2012 *Nanomaterials: Processing and Characterization with Lasers*, ed S C Singh *et al* (Weinheim: Wiley-VCH) pp 255–316
[11] Schiele N R, Corr D T, Huang Y, Raof N A, Xie Y and Chrisey D B 2010 *Biofabrication* **2** 032001
[12] Dinca V, Farsari M, Kafetzopoulos D, Popescu A, Dinescu M and Fotakis C 2008 *Thin Solid Films* **516** 6504
[13] Colina M, Serra P, Fernández-Pradas J M, Sevilla L and Morenza J L 2005 *Biosens. Bioelectron.* **20** 1638
[14] Wang J, Auyeung R C Y, Kim H, Charipar N A and Piqué A 2010 *Adv. Mater.* **22** 4462
[15] Rapp L, Diallo A K, Alloncle A P, Videlot-Ackermann C, Fages F and Delaporte P 2009 *Appl. Phys. Lett.* **95** 171109
[16] Boutopoulos C, Kalpyris I, Serpetzoglou E and Zergioti I 2014 *Microfluid. Nanofluid.* **16** 493–500
[17] Boutopoulos C, Tsouti V, Goustouridis D, Chatzandroulis S and Zergioti I 2008 *Appl. Phys. Lett.* **93** 191109
[18] Shaw Stewart J, Lippert T, Nagel M, Nüesch F and Wokaun A 2012 *Appl. Phys. Lett.* **100** 203303
[19] Duocastella M, Fernández-Pradas J M and Serra J L M P 2010 *Thin Solid Films* **518** 5321
[20] Brown M S, Brasz C F, Ventikos Y and Arnold C B 2012 *J Fluid Mech.* **709** 341
[21] Yan J, Huang Y, Xu C and Chrisey D B 2012 *J. Appl. Phys.* **112** 083105
[22] Unger C, Gruene M, Koch L, Koch J and Chichkov B N 2011 *Appl. Phys.* A **103** 271
[23] Boutopoulos C, Papageorgiou D P, Zergioti I and Papathanasiou A G 2013 *Appl. Phys. Lett.* **103** 024104
[24] Chen Y, Zhang L and Chen G 2008 *Electrophoresis* **29** 1801
[25] Gnanappa A K, Papageorgiou D P, Gogolides E, Tserepi A, Papathanasiou A G and Boudouvis A G 2012 *Plasma Processes Polym.* **9** 304
[26] Lynch D, Olson C and Weaver J 1975 *Phys. Rev.* B **11** 3617
[27] Takada N, Nakano T and Sasaki K 2009 *Appl. Surf. Sci.* **255** 9572
[28] Vogel A and Venugopalan V 2003 *Chem. Rev.* **103** 577
[29] Apitz I and Vogel A 2005 *Appl. Phys.* A **81** 329
[30] Palla-Papavlu A, Shaw-Stewart J, Mattle T, Dinca V, Lippert T, Wokaun A and Dinescu M 2013 *Appl. Surf. Sci.* **278** 180
[31] Fardel R, Nagel M, Nuesch F, Lippert T and Wokaun A 2010 *J. Phys. Chem.* C **14** 5617
[32] Hancox N and Brunton J 1966 *Phil. Trans. R. Soc.* A **260** 121
[33] Jung Y and Bhushan B 2007 *ScriptaMaterialia* **57** 1057–60
[34] Jung Y C and Bhushan B 2008 *Langmuir* **24** 6262–9
[35] Ishino C and Okumura K 2006 *Europhys. Lett. (EPL)* **76** 464–70
[36] Tsougeni K, Tserepi A, Constantoudis V, Gogolides E, Petrou P S and Kakabakos S E 2010 *Langmuir* **26** 13883
[37] Koc Y, de Mello A J, McHale G, Newton M.I, Roach P and Shirtcliffe N J 2008 *Lab Chip* **8** 582